JOURNAL OF MATERIALS SCIENCE **38** (2003) 795–802

Investigation of the graphitic microstructure in flake and spheroidal cast irons using Raman spectroscopy

C. A. COOPER, R. ELLIOTT, R. J. YOUNG*
Manchester Materials Science Centre, UMIST/University of Manchester, Grosvenor Street, Manchester, M1 7HS, UK
E-mail: robert.young@umist.ac.uk

It has been demonstrated that Raman spectroscopy is an excellent technique for the characterisation of the graphite in flake and spheroidal cast irons. The Raman spectrum of graphite is highly sensitive to both structural ordering and residual stresses as can be seen from the position, intensity and shape of the Raman bands. The relative intensities and widths of the G′ Raman bands for flake and spheroidal graphite have been compared and found to correspond to the degree of graphitisation across the graphite. The two Raman bands of the G′ doublet (G'_1 and G'_2) change in intensity and width with distance across a graphite spheroid, although their positions remain approximately constant. In contrast, the change in intensity and width of the two Raman bands of the G′ doublet for flake graphite shows no discernible pattern leading to the conclusion that there is no systematic change of graphitic ordering along a graphite flake. Finally, the fact that the positions of the G'_1 and G'_2 Raman bands for both flake and spheroidal graphite remain relatively constant with distance implies that there are no residual stresses in the graphite in flake and spheroidal cast iron.

1. Introduction

There is only one report in the literature in which the graphite phase in cast iron has been studied using Raman spectroscopy [1] where archaeological specimens of flake graphite iron were investigated and their thermal history appraised. The applicability of the Raman technique to the study of iron and steel has been discussed by Sato [2] who used the technique for the analysis of corrosion products and slags. For example, first order Raman bands in the range 298–663 cm^{-1} have been found for a variety of iron oxides such as α-FeOOH and FeO. The graphite in spheroidal irons occurs as finely dispersed spheroids and in flake irons as interconnected graphite flakes.

For flake graphite cast iron, the presence of layered rotational faults provides the means by which graphite flakes growing in preferred close-packed directions can branch in most directions within their own plane. The occurrence of certain characteristic defects in flake graphite, notably '*c*' axis rotation faults and various twin/tilt boundaries is seen to give the crystals remarkable flexibility to change orientation during growth [3]. Double and Hellawell [3] confirmed that flakes are rarely single crystals but are faulted in the planes of the graphite sheets (which are parallel to the graphite basal planes).

Double and Hellawell [3] also found that graphite spherulites have their '*c*' axes approximately parallel to the radial direction. Their close observation of the core of the spherulites sometimes revealed irregularities in the form of serrated herring-bone patterns associated with distinct curvature of the basal planes. They suggested that these irregularities could have arisen from a variety of sections though conical helices (as shown in Fig. 1). This would imply that at least near the centre of the spherulite, initial growth may begin as a loose combination of conical helices. In further studies, Double and Hellawell suggested from their findings that spherulitic graphite grows from cleaner iron melts than usual so may not nucleate upon a high density of foreign substances, but rather as a sheet or fine scroll/roll of graphite [4]. They considered that as graphite is an extended two-dimensional polymer, there is a wide range of folding and wrapping possibilities that could describe the many reported morphlogies (C_{60} and carbon nanotubes being two of the forms). They also argue that, in the presence of oxygen or sulphur, flake graphite would be the preferred form. At present there is still debate about the growth mechanism of spherulitic graphite [3–6].

2. Experimental

2.1. Materials

The flake cast iron was supplied by Forrest & Sym Foundry, Manchester and the spheroidal iron was

*Author to whom all correspondence should be addressed.

TABLE I Chemical composition (wt%) of flake and spheroidal cast iron

Cast iron	Additions (weight) %	C	Si	Mn	S	P	Mg
Flake [2]		3.2–3.4	2.0–2.5	0.6–0.8	1.5 max	0.1–0.5	–
Spheroidal [4]		3.5	2.3	0.59	0.02	0.02	0.31

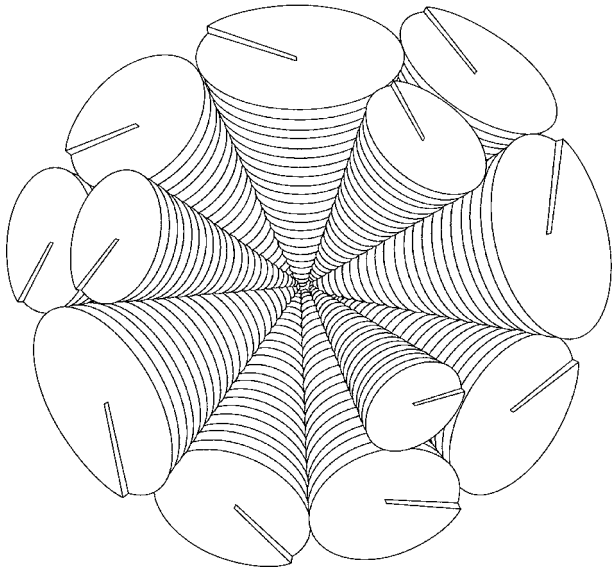

Figure 1 Schematic structural model of a graphite spheroid (After [4]).

provided by William Lee Ltd., Sheffield. Typical micro-additions to flake and spheroidal cast irons are carbon, silicon, manganese, sulphur and phosphorus with spheroidal iron also having magnesium as a spheroidiser [7]. Table I shows the chemical compositions for the flake and spheroidal iron used in this study. The cast iron specimens were prepared for optical microscopy, SEM and Raman spectroscopy by grinding the surface of the cast iron using successive grades of grinding paper (400, 600, 800, 1200 μm) followed by polishing using 6 and 1 μm polishing wheels and finally etched in 2% Nital (2 parts HNO_3 and 98 parts CH_3OH) for 10 s. The specimens were examined using an Olympus CH-2 optical microscope and a Philips XL30 Field Emission Gun Scanning Electron Microscope (FEG SEM).

2.2. Raman spectroscopy

The spectra from the carbon in the cast iron were obtained using a Renishaw 1000 Raman system employing the 633 nm red line of a 25 mW He-Ne laser with the laser beam focussed to a spot size in the order of 2 μm. Since graphite is a strong absorber of visible light the penetration depth of the laser beam is thought to be only of the order of 100 nm. The peak values were derived by using Lorentzian routines fitted to the raw Raman data obtained from the spectrometer.

3. Results and discussion

3.1. Microscopy of samples

Fig. 2a shows an optical micrograph of polished flake iron showing curved and tapering graphite flakes and the alternating layers of the cementite and ferrite of the pearlitic matrix. The variation of orientation of these layers with respect to the graphite flake axis can be seen. Fig. 2b shows an optical micrograph of polished spheroidal iron obtained using polarised light. It can be seen that the graphite crystallites radiate from a common centre.

3.2. Raman spectroscopy

Fig. 3 shows the Raman spectrum of a graphite flake and graphite nodule in the range 1000–3000 cm^{-1}. A sharp peak is seen at 1582 cm^{-1} (G band) that is characteristic of graphite structures [8, 9]. A band is seen at 1335 cm^{-1}(D band) that has been attributed to the breakdown of translational symmetry produced by the microcrystalline structure [10]. A second-order band is seen at 2673 cm^{-1} (G′ band). Significant structural information can be obtained from the Raman spectrum of graphite. The degree of graphitisation affects the relative band intensities, widths and positions [11, 12]. Moreover, the Raman bands in graphite are also sensitive to stress [12] and so the exact positions of the bands will depend upon the presence of internal stresses in the graphite.

3.2.1. Position and symmetry of the G′ Raman band position in cast iron

Examination of the G′ band in Fig. 3 reveals that it could be made up of two bands. The peak is asymmetric and fitting for two bands using a Gaussian and Lorentzian mix curve-fitting program, finds a lower frequency component at about 2654 cm^{-1}(G'_1) and a higher frequency component at around 2689 cm^{-1} (G'_2) as seen in the inset in Fig. 3.

Cuesta *et al.* [11] studied a wide range of carbon materials with a broad variation in degree of graphitisation using the 514 nm green line of an argon laser. They found that ordered carbon materials yield a well-defined band at around 2700 cm^{-1} that is split into two bands for the most graphitised solids. The position of the second order band (and the corresponding first order bands) found by Cuesta *et al.* [11], were different to that exhibited with the 633 nm He-Ne laser used in this study. The second order band position shifts by +30 cm^{-1} for a laser wavelength of 514 nm compared to the 633 nm laser line [6]. For materials with a lower level of order, a small wide band appears in the second order zone of the Raman spectrum, centred at 2900 cm^{-1}. Increased crystalline order splits the band into three: one low intensity band at 3200 cm^{-1} and two others of higher intensity at 2900 and 2700 cm^{-1}. With a continued increase in

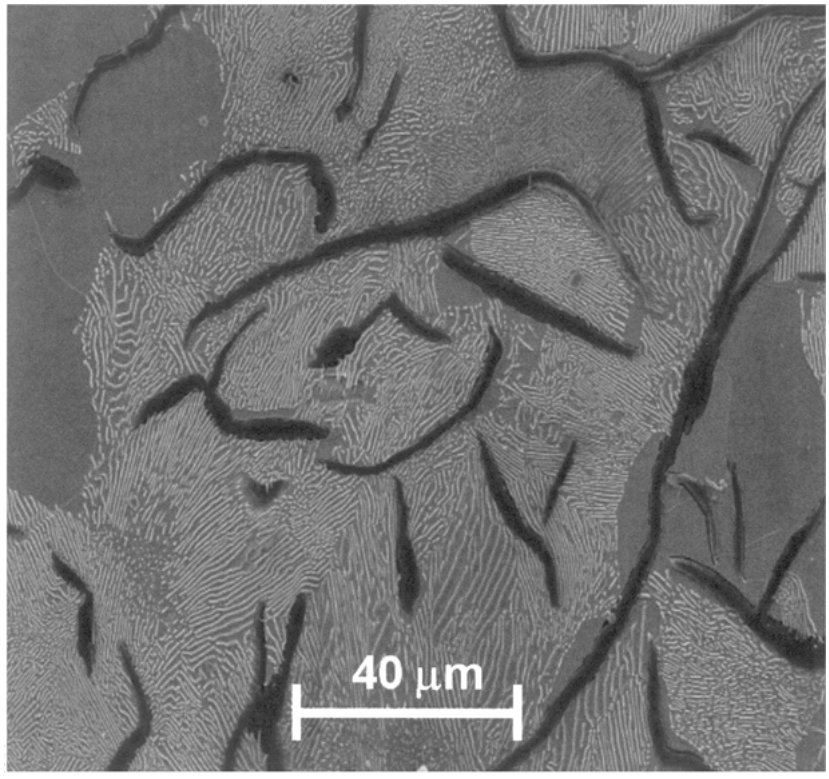

(a)

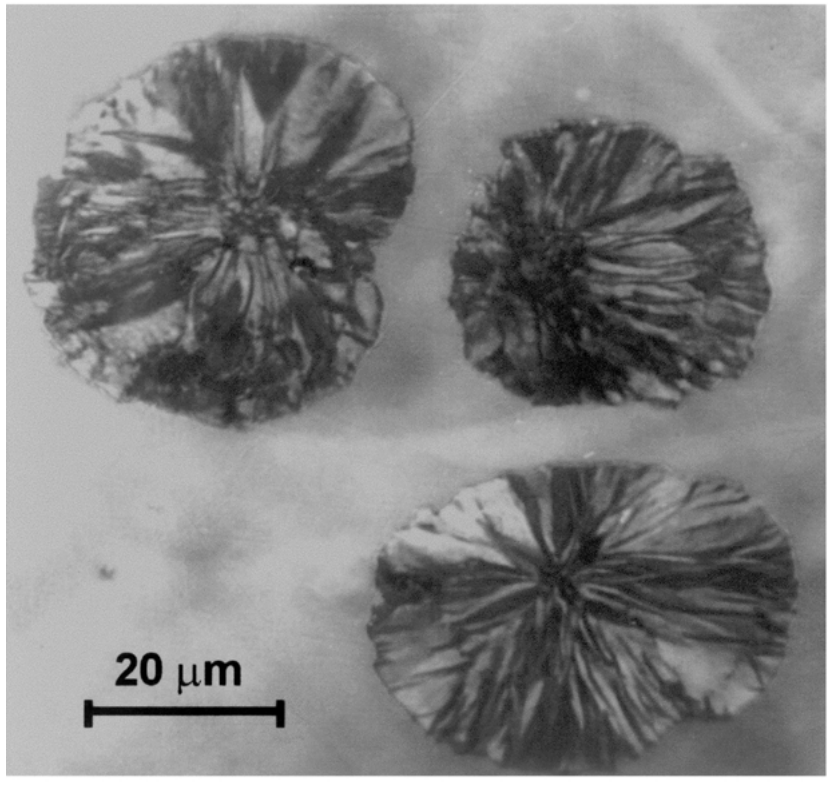

(b)

Figure 2 Optical micrographs of (a) polished and etched flake graphite iron and (b) polished spheroidal graphite iron taken with polarised light.

order, the band at 2700 cm^{-1} narrows and increases in intensity and in the final step becomes very asymmetric and even splits into two: the higher component, a sharper band, is superimposed over a wider band with lower intensity and at a lower wavenumber. This effect was seen in the cast irons investigated in this study. The evolution of graphitic ordering with the formation of the graphite flakes and spheroids was investigated by comparing the Raman spectra obtained at different positions along a graphite flake and from the central and outer regions of the spheroid. The results are discussed next.

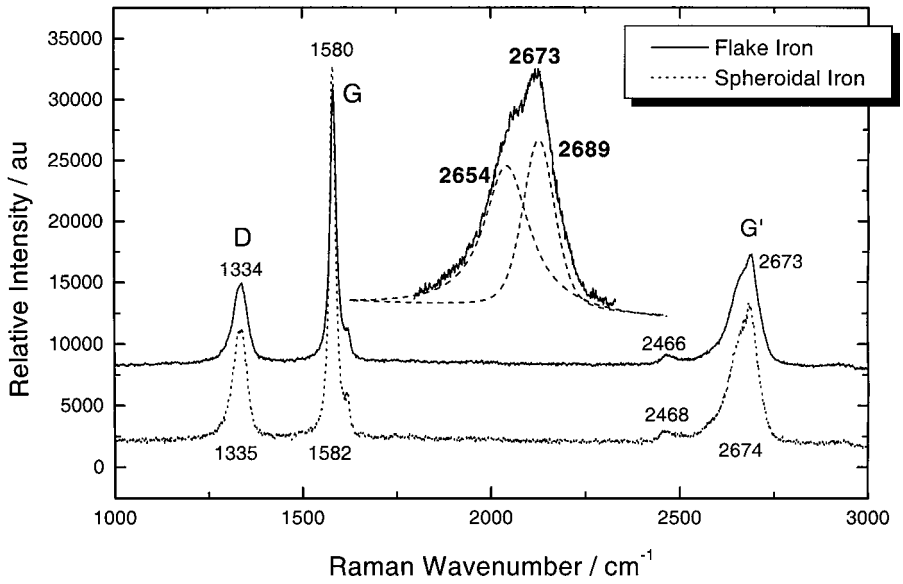

Figure 3 Raman spectrum of a graphite flake and a graphite spheroid in cast iron, inset shows the deconvolution into two peaks of the asymmetric G′ Raman band.

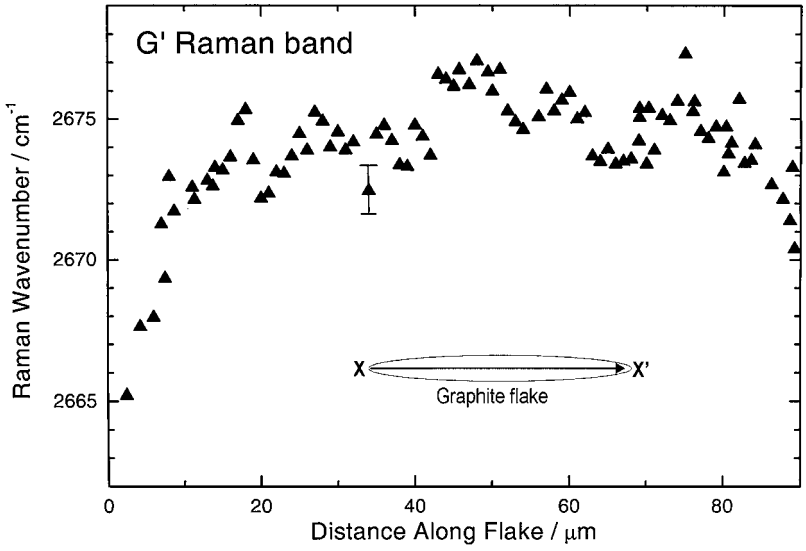

(a)

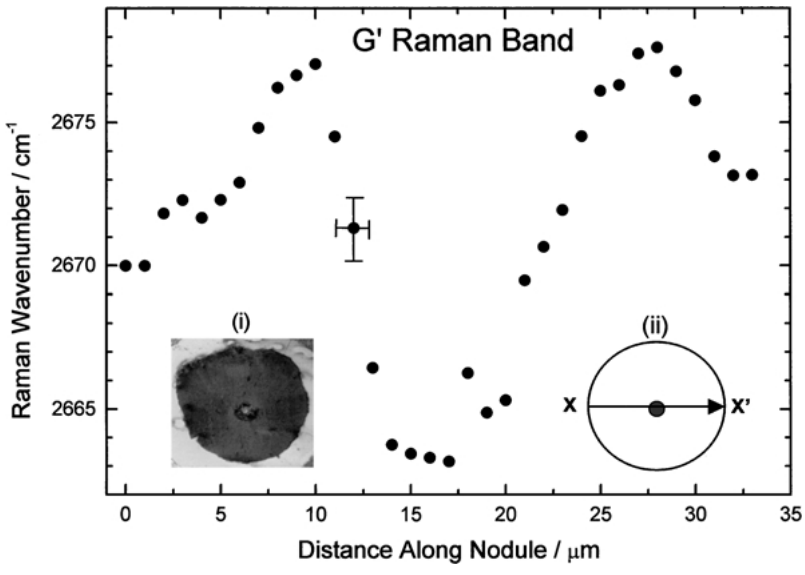

(b)

Figure 4 Variation of the G′ Raman Band position with distance (*X*–*X*′) (a) along a graphite flake in cast iron and (b) across a graphite spheroid in cast iron.

3.2.2. Variation of G′ Raman band position and shape across flake and spheroidal graphite

Raman spectra were taken at 1 μm intervals along a graphite flake and across the centre of a graphite spheroid in cast iron in the X–X' directions (as shown on the figures). The Raman spectra were obtained with the polarisation of the laser beam parallel to the X–X' direction so that any variation of residual stress along the flake axis could be determined [12]. Fig. 4a shows the variation of the G′ Raman position (fitted to a single peak) with distance along a graphite flake in cast iron. The path of the Raman mapping is shown schematically in the inset in Fig. 4a. It can be seen that although there is experimental scatter, the position of the G′ Raman band is at a lower wavenumber at the outer edges of the graphite flake than at the centre.

It was observed that some graphite nodules in the cut and polished samples had a small discoloured central region. Such discoloured regions could be oxide, sulphide or oxysulphide inclusions. This was seen when the spheroid was sectioned directly through the equatorial region. A discoloured region can be seen in the centre of the spheroid shown in the inset (i) in Fig. 4b and schematically in the inset (ii) in Fig. 4b. To determine whether there was any change in graphite ordering from the perimeter to the central region, Raman spectra were taken at 1 μm intervals along the diameter of the spheroid section with the polarisation in the radial direction again to detect any radial residual stresses.

It can be seen from Fig. 4b that the position of the G′ Raman band (fitted to a single peak) shifts to a higher frequency with distance away from the initial lower edge position. In the vicinity of the spheroid nucleus however, the G′ band position decreased rapidly to a minimum at 2663 cm^{-1} at the centre of the nucleus. This decrease of about 14 cm^{-1} could be due to structural disordering of the graphite in the very centre of the nodule. The decrease in the G′ Raman band position in the central region was investigated further by comparing the shape of the G′ Raman peak obtained from the vicinity of the graphite nucleus region.

Fig. 5 shows that the intensity of the G′ Raman band for the graphite spheroid increases noticeably in the centre of the nucleus. Tsu [13] found that the intensity of the 1334 cm^{-1} band grew with disorder and the band tended to become narrower as it grew, suggesting that the density of states also becomes sharper, also indicating that distortion of the crystal structure is also involved. Fig. 5 also shows that the intensities of the two G′ band peaks (G'_1 and G'_2) change relative to each other and that the overall shape of the band changes from being very asymmetric to being a sharp narrow peak. This dramatic change in shape of the G′ Raman band was not observed with the Raman mapping along graphite flakes in cast iron.

3.3. Variation in G'_1 and G'_2 intensities and positions across a graphite flake and spheroid in cast iron

The G′ doublet was fitted for two peaks using a mixed Gaussian and Lorentzian fitting routine. This was performed for the same graphite flake analysed in Fig. 4a and graphite spheroid analysed in Figs 4b and 5.

3.3.1. G'_1 and G'_2 Raman band intensities

It can be seen from Fig. 6a that the variation in peak intensity of the G'_1 Raman band along the graphite flake. The G'_2 peak intensity decreases from the edges of the flake, then increases towards the centre and finally

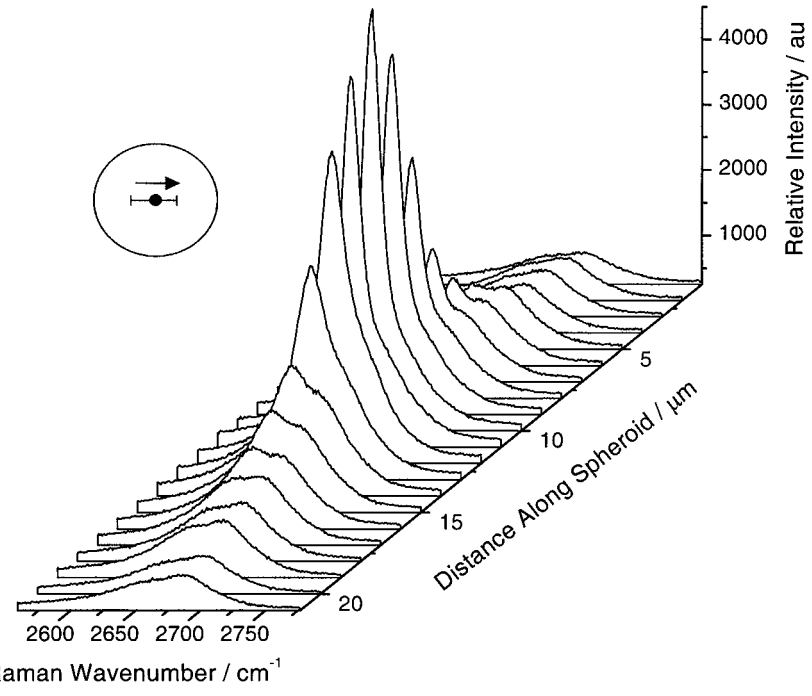

Figure 5 Change in the intensity and shape of the G′ Raman band with distance across a graphite spheroid in cast iron.

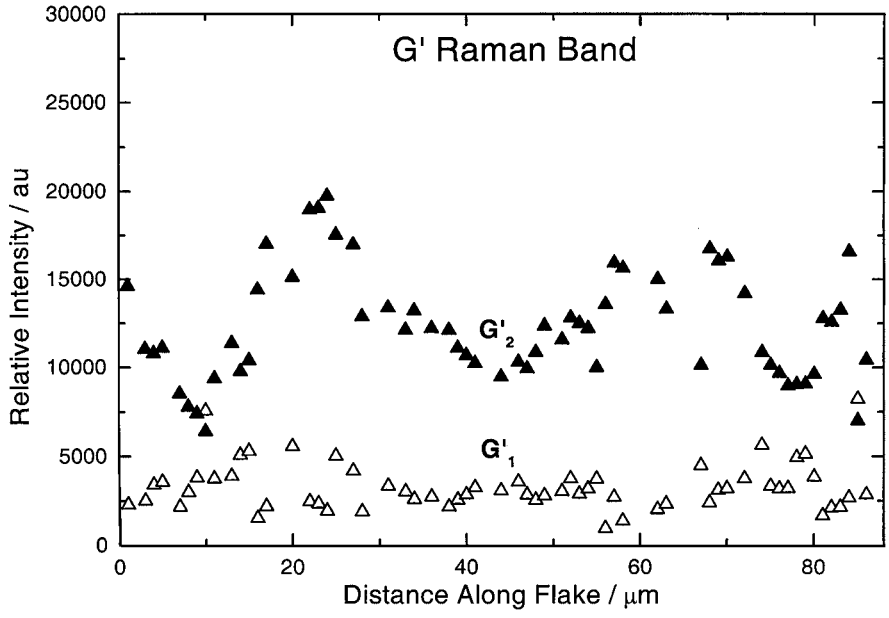

(a)

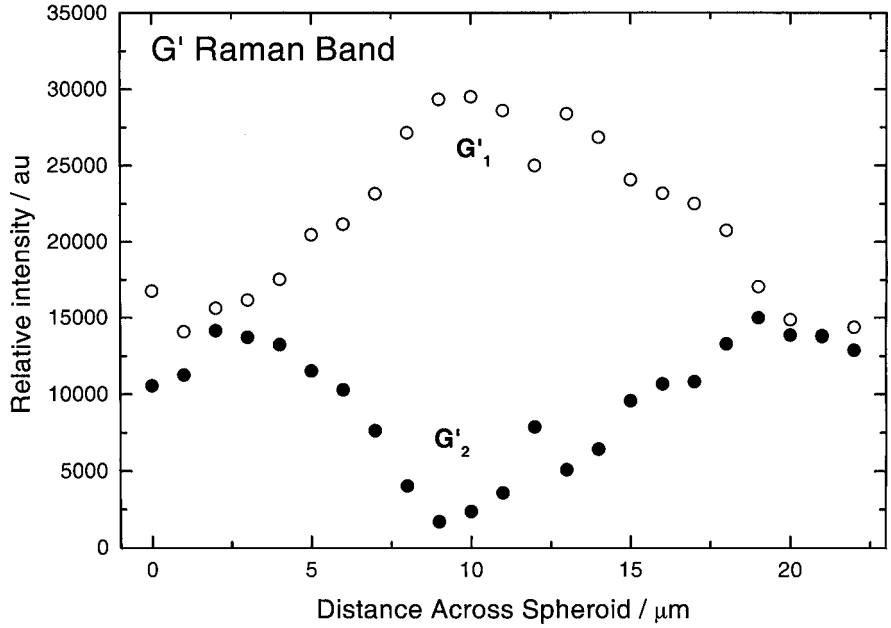

(b)

Figure 6 Variation of the G'_1 and G'_2 intensities with distance (X–X') (a) along a graphite flake in cast iron and (b) across a graphite spheroid in cast iron.

decreases again at the centre of the flake. In contrast, there is a large systematic variation in both the G'_1 and G'_2 band intensities across the graphite spheroid as can be seen in Fig. 6b. The G'_1 band intensity increases towards the centre of spheroid and then decreases again with distance away from the nucleus. The G'_2 band shows the opposite behaviour with the intensity decreasing towards the centre of the spheroid.

3.3.2. G'_1 and G'_2 Raman peak positions

Fig. 7a shows the variation of the separate peak positions for the G'_1 and G'_2 Raman bands along a graphite flake in cast iron. It can be seen that there is a little experimental scatter in the position of these two bands but the overall Raman band positions vary very little along the graphite flake. Fig. 7b shows the variation of the peak positions for the G'_1 and G'_2 Raman bands across a graphite spheroid in cast iron. It can be seen again that there is very little variation in the position of these two bands. Hence it appears that there are no residual stresses in the graphite. Although a relationship between the D and G band intensities has been found by other workers [11, 13, 14], the effect of the structural ordering on the G'_1 and G'_2 band intensities on graphite in cast iron has not been fully investigated up to now.

The data in Fig. 4 show that when the G' band is fitted to a single peak its position appears to vary across the microstructure, implying that there might be residual stresses in the graphite. However, the analysis described

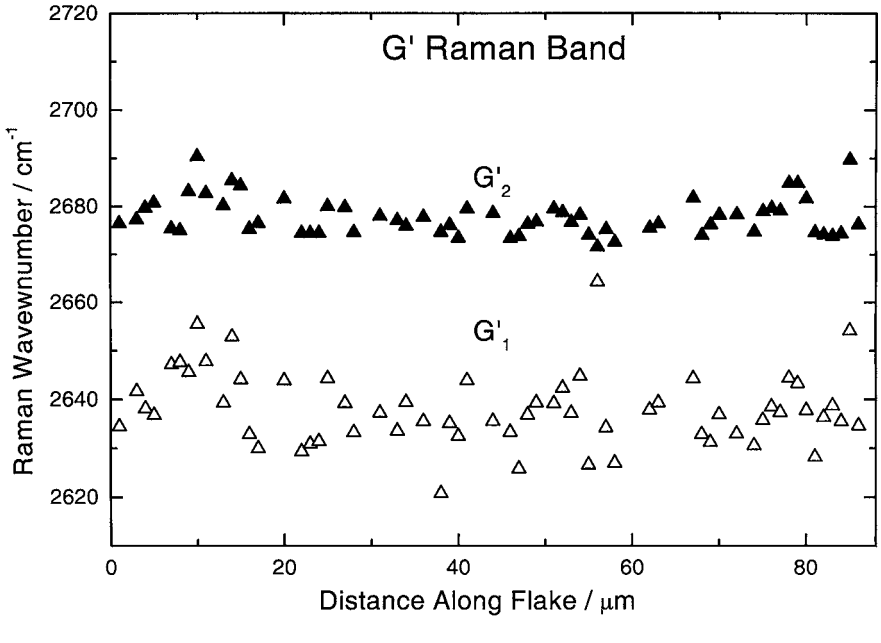

(a)

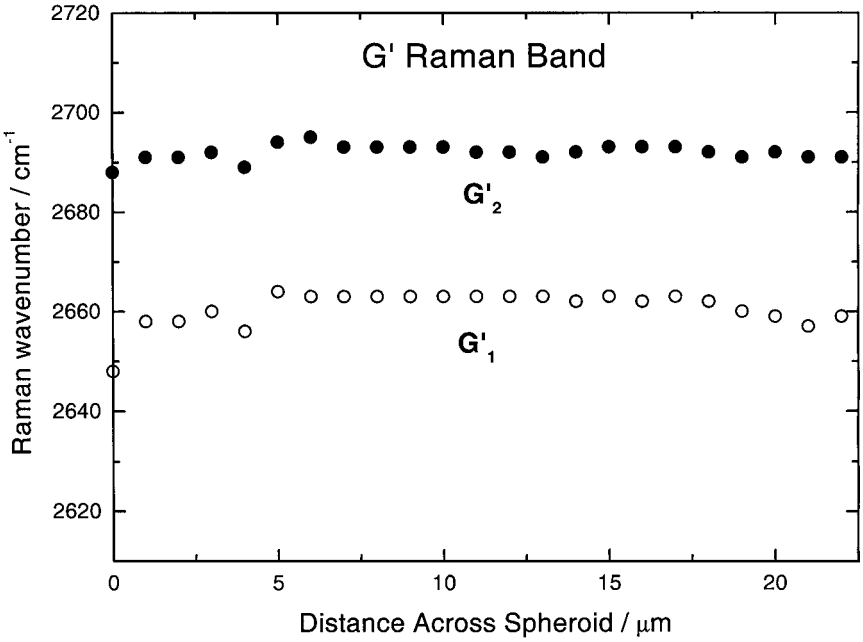

(b)

Figure 7 Variation of the G'_1 and G'_2 Raman band positions with distance (X–X') (a) along a graphite flake in cast iron and (b) across a graphite spheroid in cast iron.

above shows that the apparent peak shift is due to changes in the relative intensity of the G'_1 and G'_2 bands as a result of variations in the graphite microstructure.

4. Conclusions

It has been demonstrated that Raman spectroscopy can be used to characterise the graphite in two different forms of cast iron. It has been found for the flake and spheroidal graphite in cast iron, that the shape, positions and intensities of the G′ Raman band and the two peaks of the G′ band doublet indicate ordering that can be related to the growth mechanisms of the graphite. The two Raman bands of the G′ doublet change significantly in intensity with distance across a graphite spheroid, although their positions remain approximately constant. In contrast, the intensities of the two Raman bands of the G′ doublet for flake graphite are relatively constant leading to the conclusion that there is no systematic change of graphitic ordering along a graphite flake. Finally, the fact that the positions of the doublet G'_1 and G'_2 Raman bands for both flake and spheroidal graphite remained relatively constant across the microstructure implies that there are no significant residual stresses in the graphite in these cast irons.

Acknowledgments

The authors would like to thank Forrest and Sym Foundry, Manchester for supplying the flake graphite iron and William Lee Ltd., Sheffield. for supplying the

spheroidal graphite iron used in this study. This work is part of a larger programme supported by the EPSRC.

References

1. C. HIRLIMANN, M. JOUANNE and C. FORRIÉRES, *J. Raman Spectroscopy* **23** (1992) 315.
2. K. SATO, *Transactions of the Iron and Steel Industry* **21** (1981) 370.
3. D. D. DOUBLE and A. HELLAWELL, *Acta Metall.* **22** (1974) 481.
4. *Idem.*, *Acta. Metall. Mater.* **43** (1995) 2435.
5. B. MIAO, D. O. N. WOOD, W. BIAN, K. FANG and M. H. FAN, *J. Mater. Sci.* **29** (1994) 255.
6. Website 'A New Approach to the Solidification of Ductile Cast Iron,' http://members.tripod.lycos.nl/cvdv/index.html.
7. R. ELLIOTT, "Cast Iron Technology" (Butterworths, 1988).
8. Y. HUANG and R. J. YOUNG, *Carbon* **33** (1995) 97.
9. R. J. NEMANICH and S. A. SOLIN, *Solid State Communications* **23** (1977) 417.
10. *Idem.*, *Physical Review* B **20** (1979) 392.
11. A. CUESTRA, P. DHAMELINCOURT, J. LAUREYNS, A. MARTÍNEZ-ALONSO and J. M. D. TASCÓN, *Carbon* **32** (1994) 1523.
12. R. J. YOUNG, *J. Text. Inst.* **86** (1995) 360.
13. R. TSU, J. H. GONZÁLEZ and I. C. HERNÁNDEZ, *Solid St. Comm.* **27** (1978) 507.
14. K. ANGONI, *Carbon* **31** (1993) 537.

Received 10 January
and accepted 31 October 2002